Analysis of Kinematics and Dynamics Performance of a New Type of Three-Pronged Sliding Universal Coupling

Xia Xiu , Degong Chang , Yunpeng Ju * , Liang Zheng

Posted Date: 5 March 2024

doi: 10.20944/preprints202403.0252.v1

Keywords: Three fork type universal coupling; Kinematics; Dynamic performance; The optimal operating angle range

Article

Analysis of Kinematics and Dynamics Performance of a New Type of Three-Pronged Sliding Universal Coupling

Xia Xiu [1], Degong Chang [2], Yunpeng Ju [2,*] and Liang Zheng [2]

[1] Heng Xing University, Qingdao 266100, China; xiaxia0208521@163.com
[2] Qingdao University of Science and Technology, Qingdao 266061, China; hyg867@163.com; 2459785416@qq.com
* Correspondence: Yunpeng Ju (e-mail: xitilei@163.com)

Abstract: The three-pronged sliding universal coupling is a new kind of three-pronged coupling. To study its kinematic and dynamic characteristics, directional cosine matrices are utilized as tools to analyze the coordinate systems by establishing simplified geometric models and corresponding motions. Through the analysis of the motions of the input and output shafts and employing the method of single-force element, a set of equilibrium equations for the forces acting on the output shaft and the input shaft are formulated for solution analysis. The research indicates that during the rotation process, there exists a small angular difference between the input shaft and the intermediate shaft, demonstrating the quasi-constant angular velocity characteristics of the new tripod sliding universal coupling. The curves of the forces and torques acting on each component of the coupling approximate sinusoidal curves. The optimal operating angle range for the new tripod universal coupling is at angle $\beta \leq 25^0$, during which the system exhibits good transmission and mechanical performance.

Keywords: three fork type universal coupling; kinematics; dynamic performance; the optimal operating angle range

1. Introduction

Couplings are commonly used mechanical transmission components, primarily employed to connect two shafts or a connecting shaft with other rotating components in various mechanisms. Their purpose is to enable the synchronized rotation of these shafts and facilitate the transmission of motion and torque [1–3]. Among them, universal joint couplers can be applied in situations where there is a significant angular deviation between two shafts, and they can continue to be used even when the angle changes [4–6]. Common universal joint couplers can be classified into three forms based on their motion characteristics: non-constant velocity universal joint couplers, quasi-constant velocity universal joint couplers, and constant velocity universal joint couplers [7,8].

The novel triple-rod sliding universal joint coupler is a new type of three-rod coupler invented by our research team [9–11], as shown in Figure 1. It mainly consists of a triple-rod sleeve, three sliding pin rods, three inner bearings, and the triple rod itself. Among them, The inner bearing can rotate relatively freely, forming a spherical pair; the sliding pin rod can slide relative to the triple-rod sleeve hole and is connected to the inner bearing. Compared to traditional triple-rod roller-type couplers, the triple-rod sliding universal joint coupler uses three sliding pin rods instead of three spherical or cylindrical rollers. This design allows it to transmit larger torques. Additionally, its structure is simpler, and it comes with advantages such as easy installation, low manufacturing cost, and high transmission efficiency. It can be widely applied in situations requiring heavy torque and heavy loads. By using three sliding pin rods instead of three spherical or cylindrical rollers, the triple-

 doi:10.20944/preprints202403.0252.v1

rod sliding universal joint coupler improves upon the original triple-rod roller-type coupler, which suffered from high contact stress and significant wear due to small contact areas.

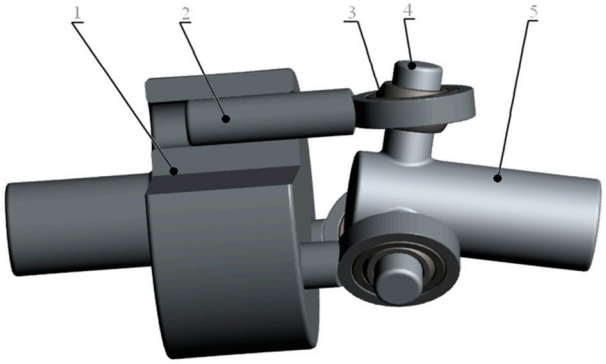

Figure 1. Tripod universal joint assembly 1-input shaft, 2- slide-rod, 3-joint bearing, 4-tripod arm, 5-tripod.

The new type of triple-rod sliding universal joint coupler can be widely used in transmission systems, especially in the automotive industry, with broad prospects for application [12]. Therefore, conducting kinematic and dynamic performance analysis on it is of significant importance, paving the way for further applications in various fields. To achieve precise analysis of the coupling, it is necessary to clearly define the composition of the coupling before conducting relevant research. Based on this, establish the motion equations for the three-pronged universal coupling [13]. To understand the motion characteristics of universal couplings and further clarify the motion laws of this device, design an analysis method specifically for this device, focusing on the three-pronged universal coupling as the research object [14]. This article utilizes the direction cosine matrix to analyze the motion of the input and output shafts, studying the effects of the angle between the axes of the input and output shafts and the rotational frequency of the coupler on the motion of the sliding pin rod within the triple-rod sleeve holes. Building upon this motion analysis, the single force method is employed [15–17] to establish the force equilibrium equations for the output shaft and the input end shaft, followed by solving and analyzing these equations to delve into the dynamic behavior of the input and output shafts. In the dynamic analysis, the use of the single force method bypasses the need for complex solving processes. This method is a straightforward and intuitive approach to force analysis, where the focus lies not on simultaneously determining all constraint forces but rather on initially calculating the constraint forces within a specific motion pair. Subsequently, the equilibrium equations for the remaining motion pairs are solved individually, component by component.

2. Establishment of Motion, Force Diagram, and Coordinate System

The coordinate system as illustrated in Figure 2 and Figure 3 [18] is employed: Two fixed coordinate systems, $oxyz$ and $O'X'Y'Z'$, are taken. The centerline of the output shaft rotary cone and the axis of the input shaft are designated as axes oz and $O'Z'$, respectively. Axis oy coincides with axis $O'Y'$, perpendicular to axes oz and $O'Z'$, forming angle β. Furthermore, at the intersection of the three-bar linkage, an auxiliary coordinate system $O''X''Y''Z''$ is established with axis $O''Z''$ aligned with the output shaft, and plane $X''O''Y''$ representing the plane of the three-bar linkage, with axis $O''Y''$ always perpendicular to axis ox. In the initial configuration, it is assumed that the axis m_1 of the plunger groove lies in plane $X'O'Z'$, while the connecting rod n_1 lies in the moving plane $X''O''Z''$ that coincides with the fixed plane xoz. When the input shaft

Preprints.org (www.preprints.org) | NOT PEER-REVIEWED | Posted: 5 March 2024 doi:10.20944/preprints202403.0252.v1

passes through any point φ_1, the connecting rod n_1 on the output shaft rotates by a corresponding angle φ_0 around the output shaft.

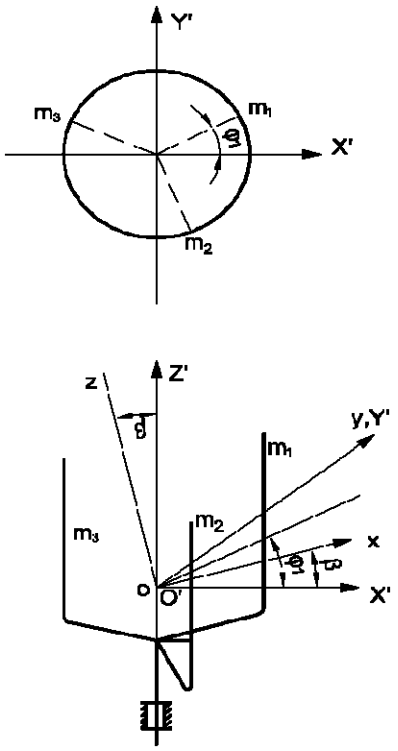

Figure 2. The position of the input axis in the coordinate system($O'X'Y'Z'$) at the angle(φ_1) of rotation.

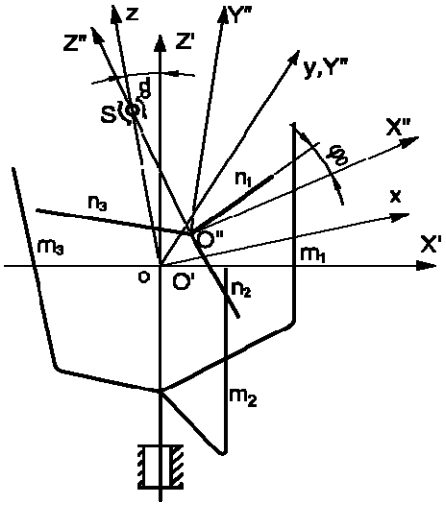

Figure 3. Coordinate system for motion analysis when the output shaft is installed with aligning bearings.

In the given scenario, m_1, m_2, m_3 refer to the axis of the plunger groove, while n_1, n_2, n_3 represent the axis of the connecting rod. It is known that there is no relative sliding between the output shaft and the inner ring of the self-aligning bearing. The distance from the intersection of the three-bar linkage to the center of the self-aligning bearing, denoted as l, remains constant. The motion of the output shaft is a conical motion with a cone angle of θ. The radius of the motion

Preprints.org (www.preprints.org) | NOT PEER-REVIEWED | Posted: 5 March 2024 doi:10.20944/preprints202403.0252.v1

trajectory of the center of the three-bar linkage is ρ. The angle between the center lines of the input shaft and the output shaft is β. The distance from the axis of the plunger groove to the axis of the input shaft is r. The distance between the center of the ball joint and the center of the connecting rod is h.

3. Kinematic Analysis

The unified expression of the three plunger groove axes m_1, m_2, m_3 in coordinate system $O'X'Y'Z'$ is:

$$\begin{cases} X' = r\cos\left[\varphi_1 + (j-1)\dfrac{2}{3}\pi\right] \\ Y' = r\sin\left[\varphi_1 + (j-1)\dfrac{2}{3}\pi\right] \end{cases} \quad (j = 1,2,3) \tag{1}$$

Utilizing the following coordinate transformations

$$\begin{bmatrix} X' \\ Y' \\ Z' \end{bmatrix} = \begin{bmatrix} \cos\beta & 0 & -\sin\beta \\ 0 & 1 & 0 \\ \sin\beta & 0 & \cos\beta \end{bmatrix} \begin{bmatrix} x \\ y \\ z \end{bmatrix} \tag{2}$$

Transformed into coordinate system $oxyz$

$$\begin{cases} x\cos\beta - z\sin\beta = r\cos\left[\varphi_1 + (j-1)\dfrac{2}{3}\pi\right] \\ y = r\sin\left[\varphi_1 + (j-1)\dfrac{2}{3}\pi\right] \end{cases} \quad (j = 1,2,3) \tag{3}$$

The expression of the axes n_1, n_2, n_3 of the three-rod in the moving coordinate system $O''X''Y''Z''$, in the fixed coordinate system $oxyz$, can be referred to as shown in Figure 4.

$$\begin{cases} Y'' = X''tg\left[\varphi_0 + (j-1)\dfrac{2}{3}\pi\right] \\ Z'' = 0 \end{cases} \quad (j = 1,2,3) \tag{4}$$

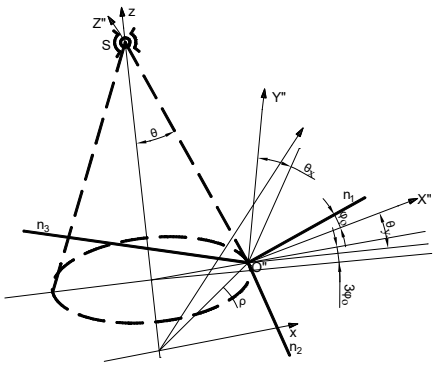

Figure 4. Rotation the angle(φ_0) of the axis($O''Z''$) of the three-prong rod in the moving coordinate system($O''X''Y''Z''$).

Preprints.org (www.preprints.org) | NOT PEER-REVIEWED | Posted: 5 March 2024 doi:10.20944/preprints202403.0252.v1

The coordinates of the origin O'' of the moving coordinate system $O''X''Y''Z''$ in the fixed coordinate system $oxyz$ can be determined by referencing Figure 4.

$$\begin{cases} X^{(O'')} = \rho\cos\theta\sin 3\varphi_0 \\ Y^{(O'')} = \rho\cos\theta\cos 3\varphi_0 \\ Z^{(O'')} = \rho\sin\theta \end{cases} \tag{5}$$

Since the $O''Y''$ axis of the moving coordinate system $O''X''Y''Z''$ is always perpendicular to the ox axis of the fixed coordinate system, it can be considered that, as shown in Figure 2: first, rotate the $oxyz$ coordinate system about the ox axis by an angle θ_x to align the oy axis parallel to the $O''Y''$ axis, then rotate about the new oy axis by an angle θ_y to align the x axis parallel to $O''X''$, while also making the oz axis parallel to the $O''Z''$ axis.

Due to the transformation relationship between the fixed coordinate system and the moving coordinate system $O''X''Y''Z''$.

$$\begin{bmatrix} x \\ y \\ z \end{bmatrix} = \begin{bmatrix} \rho\cos\theta\sin 3\varphi_0 \\ \rho\cos\theta\cos 3\varphi_0 \\ \rho\sin\theta \end{bmatrix} + \begin{bmatrix} 1 & 0 & 0 \\ 0 & \cos\theta_x & -\sin\theta_x \\ 0 & \sin\theta_x & \cos\theta_x \end{bmatrix} \begin{bmatrix} \cos\theta_y & 0 & \sin\theta_y \\ 0 & 1 & 0 \\ -\sin\theta_y & 0 & \cos\theta_y \end{bmatrix} \begin{bmatrix} X'' \\ Y'' \\ Z'' \end{bmatrix} \tag{6}$$

Based on the properties of matrix transformations

$$\begin{bmatrix} X'' \\ Y'' \\ Z'' \end{bmatrix} = \begin{bmatrix} \cos\theta_y & \sin\theta_x\sin\theta_y & -\cos\theta_x\sin\theta_y \\ 0 & \cos\theta_x & \sin\theta_x \\ \sin\theta_y & -\sin\theta_x\cos\theta_y & \cos\theta_x\cos\theta_y \end{bmatrix} \begin{bmatrix} x \\ y \\ z \end{bmatrix} - \begin{bmatrix} \rho\cos\theta\sin 3\varphi_0 \\ \rho\cos\theta\cos 3\varphi_0 \\ \rho\sin\theta \end{bmatrix} \tag{7}$$

After expanding

$$\begin{cases} X'' = x\cos\theta_y + y\sin\theta_x\sin\theta_y - z\cos\theta_x\sin\theta_y - \rho\cos\theta\sin 3\varphi_0 \\ Y'' = y\cos\theta_x + z\sin\theta_x - \rho\cos\theta\cos 3\varphi_0 \\ Z'' = x\sin\theta_y - y\sin\theta_x\cos\theta_y + z\cos\theta_x\cos\theta_y - \rho\sin\theta \end{cases} \tag{8}$$

The angles θ_x and θ_y can be determined by the intersection point S of axes oz and $O''Z''$. By substituting the coordinates of point S in both coordinate systems, $(0,0,l/\cos\theta)$ and $(0,0,l)$, into the above equation, θ_x and θ_y can be solved.

$$\theta_x = arc\sin\left(\frac{\rho}{l}\cos^2\theta\cos 3\varphi_0\right) \tag{9}$$

$$\theta_y = arc\cos\left(\frac{\rho\sin\theta\cos\theta}{\sqrt{l^2 - \rho^2\cos^4\theta\cos^2(3\varphi_0)}}\right) \tag{10}$$

Substitute equation (8) into equation (4), then after simplification, the equation of the axis of the three rods (Rod n_1, Rod n_2, Rod n_3) in the $oxyz$ coordinate system can be obtained.

 doi:10.20944/preprints202403.0252.v1

$$\begin{cases} x\cos\theta_y tg\varphi_0 + y\left(\sin\theta_x \sin\theta_y tg\varphi_0 - \cos\theta_y\right) - z\left(\cos\theta_x \sin\theta_y tg\varphi_0 + \sin\theta_x\right) \\ = \rho\cos\theta\sin 3\varphi_0 tg\varphi_0 - \rho\cos\theta\cos 3\varphi_0 \\ x\sin\theta_y - y\sin\theta_x\cos\theta_y + z\cos\theta_x\cos\theta_y = \rho\sin\theta \end{cases} \tag{11}$$

$$\begin{cases} x\cos\theta_y tg\left(\varphi_0 + \frac{2}{3}\pi\right) + y\left[\sin\theta_x \sin\theta_y tg\left(\varphi_0 + \frac{2}{3}\pi\right) - \cos\theta_y\right] \\ -z\left[\cos\theta_x \sin\theta_y tg\left(\varphi_0 + \frac{2}{3}\pi\right) + \sin\theta_x\right] \\ = \rho\cos\theta\sin 3\left(\varphi_0 + \frac{2}{3}\pi\right) tg\left(\varphi_0 + \frac{2}{3}\pi\right) - \rho\cos\theta\sin 3\left(\varphi_0 + \frac{2}{3}\pi\right) \\ x\sin\theta_y - y\sin\theta_x\cos\theta_y + z\cos\theta_x\cos\theta_y = \rho\sin\theta \end{cases} \tag{12}$$

$$\begin{cases} x\cos\theta_y tg\left(\varphi_0 + \frac{4}{3}\pi\right) + y\left[\sin\theta_x \sin\theta_y tg\left(\varphi_0 + \frac{4}{3}\pi\right) - \cos\theta_y\right] \\ -z\left[\cos\theta_x \sin\theta_y tg\left(\varphi_0 + \frac{4}{3}\pi\right) + \sin\theta_x\right] \\ = \rho\cos\theta\sin 3\left(\varphi_0 + \frac{4}{3}\pi\right) tg\left(\varphi_0 + \frac{4}{3}\pi\right) - \rho\cos\theta\cos 3\left(\varphi_0 + \frac{4}{3}\pi\right) \\ x\sin\theta_y - y\sin\theta_x\cos\theta_y + z\cos\theta_x\cos\theta_y = \rho\sin\theta \end{cases} \tag{13}$$

To determine the relationship between the input shaft angle φ_1 and the output shaft angle φ_0, we can utilize the characteristic that the axis of the plunger slot m_1 should intersect with the rod n_1. Therefore, we can express this by utilizing equations (3) and (11).

$$\begin{cases} A_1 x + B_1 y + C_1 z + D_1 = 0 \\ A_1' x + B_1' y + C_1' z + D_1' = 0 \\ A_1'' x + B_1'' y + C_1'' z + D_1'' = 0 \\ A_1''' x + B_1''' y + C_1''' z + D_1''' = 0 \end{cases} \tag{14}$$

Among which

$A_1 = \cos\beta \quad B_1 = 0 \quad C_1 = -\sin\beta \quad D_1 = -r\cos\varphi_1$

$A_1' = 0 \quad B_1' = 1 \quad C_1' = 0 \quad D_1' = -r\sin\varphi_1$

$A_1'' = \cos\theta_y tg\varphi_0 \quad B_1'' = \sin\theta_x \sin\theta_y tg\varphi_0 - \cos\theta_y \quad C_1'' = -\cos\theta_x \sin\theta_y tg\varphi_0 - \sin\theta_x$

$D_1'' = -\rho\cos\theta\sin 3\varphi_1 tg\varphi_0 + \rho\cos\theta\cos 3\varphi_0$

$A_1''' = \sin\theta_y \quad B_1''' = \sin\theta_x\cos\theta_y \quad C_1''' = \cos\theta_x\cos\theta_y \quad D_1''' = \rho\sin\theta$

According to equation (14), a solution exists, so the condition must be satisfied.

 doi:10.20944/preprints202403.0252.v1

$$\begin{vmatrix} A_1 & B_1 & C_1 & D_1 \\ A_1' & B_1' & C_1' & D_1' \\ A_1'' & B_1'' & C_1'' & D_1'' \\ A_1''' & B_1''' & C_1''' & D_1''' \end{vmatrix} = 0 \tag{15}$$

Substitute each coefficient into equation (15), expand it, and obtain a complex relationship involving arbitrary angular variables φ_1 and φ_0. It can be written in the following form:

$$A(\varphi_0)\sin\varphi_1 + B(\varphi_0)\cos\varphi_1 + C(\varphi_0) = 0 \tag{16}$$

Suppose:

$$\begin{aligned} A(\varphi_0) = r\Big[&\cos\beta\left(\sin\theta_x\sin\theta_y tg\varphi_0 - \cos\theta_y\right)\cos\theta_x\cos\theta_y + \sin\beta\cos\theta_y tg\varphi_0\sin\theta_x\cos\theta_y \\ &+\sin\theta_y\left(\sin\theta_x\sin\theta_y tg\varphi_0 - \cos\theta_y\right)\sin\beta \\ &-\sin\theta_x\cos\theta_y\left(\cos\theta_x\sin\theta_y tg\varphi_0 + \sin\theta_x\right)\cos\beta\Big] \\ B(\varphi_0) = r\Big[&\cos\theta_y tg\varphi_0\cos\theta_x\cos\theta_y + \sin\theta_y\left(\cos\theta_x\sin\theta_y tg\varphi_0 + \sin\theta_x\right)\Big] \\ C(\varphi_0) = \cos\beta\Big[&\rho\sin\theta\left(\cos\theta_x\sin\theta_y tg\varphi_0 + \sin\theta_x\right) - \cos\theta_x\cos\theta_y\left(\rho\cos\theta\sin 3\varphi_0 tg\varphi_0\right. \\ &\left.+\rho\cos\theta\cos 3\varphi_0\right)\Big] + \sin\beta\Big[\rho\sin\theta\cos\theta_y tg\varphi_0 \\ &+\sin\theta_y\left(\rho\cos\theta\sin 3\varphi_0 tg\varphi_0 + \rho\cos\theta\cos 3\varphi_0\right)\Big] \end{aligned}$$

Citation for the half-angle formula can be obtained as follows:

$$\varphi_1 = 2arctg\frac{A\left(\varphi_0 \pm \sqrt{A^2(\varphi_0) + B^2(\varphi_0) - C^2(\varphi_0)}\right)}{B(\varphi_0) - C(\varphi_0)} \tag{17}$$

From this, the functional relationship between the input angle φ_1 and the output angle φ_0 can be obtained.

When r/l is small, we can assume that $\rho/l = tg\theta \approx \sin\theta \approx \theta$, or in other words, point O'' lies within the $oxyz$ coordinate plane. At the same time, terms containing r/l or ρ/l squared, as well as higher-order terms, can be neglected. Thus, we have the following simplified calculation relationship:

$$\varphi_0 - \varphi_1 \approx \frac{r(1-\cos\beta)}{2l(1+\cos\beta)} tg\beta\cos 3\varphi_1 \tag{18}$$

$$\frac{d\varphi_0}{d\varphi_1} = w_0 / w_1 = 1 - \frac{3r(1-\cos\beta)}{2l(1+\cos\beta)} tg\beta\cos 3\varphi_1 \tag{19}$$

The theoretical angular deviation curve calculated according to equation (18) is shown in Figure 5. From equation (18), it can be seen that the angular deviation varies with the deflection angle β. When the input shaft rotates one turn, the angular deviation undergoes three cycles of variation. At the deflection angle 10^0, only a fraction of the maximum angular deviation occurs at point 1'; even when the deflection angle is 30^0, the maximum angular deviation does not exceed $10'$. The curve

Preprints.org (www.preprints.org) | NOT PEER-REVIEWED | Posted: 5 March 2024 doi:10.20944/preprints202403.0252.v1

of maximum angular deviation varies with the deflection angles β and $\lambda = \frac{r}{l}$ as shown in Figure 6.

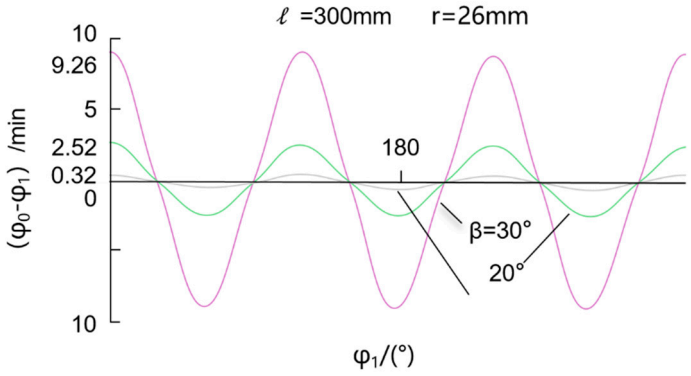

Figure 5. According to equation (23), the relation curve between the φ_1 angle difference and the value is calculated.

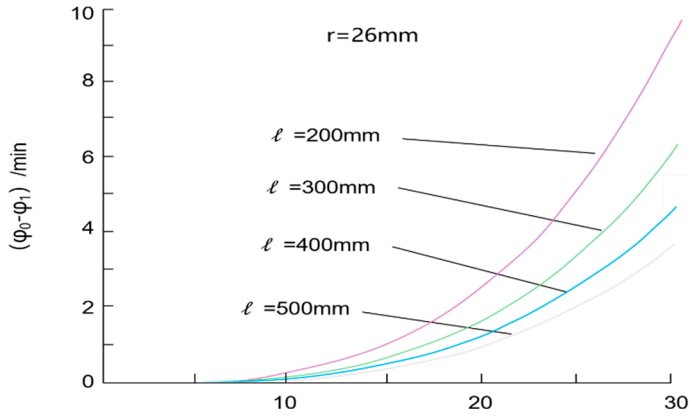

Figure 6. Change curve of Angle difference with the β angle of deflection when aligning bearing is used for three-prong type universal coupling.

4. Dynamics Analysis

The dynamic analysis of the new type of three-rod sliding constant-velocity universal joint is based on the motion analysis. The purpose of force analysis is to determine the support forces and support moments at various support points, thereby establishing the mechanical performance of this type of coupling. Here, let's assume an idealized condition, neglecting friction and gravity. The force diagram for the three-rod sliding constant-velocity universal joint with self-aligning bearings is illustrated in Figure 7.

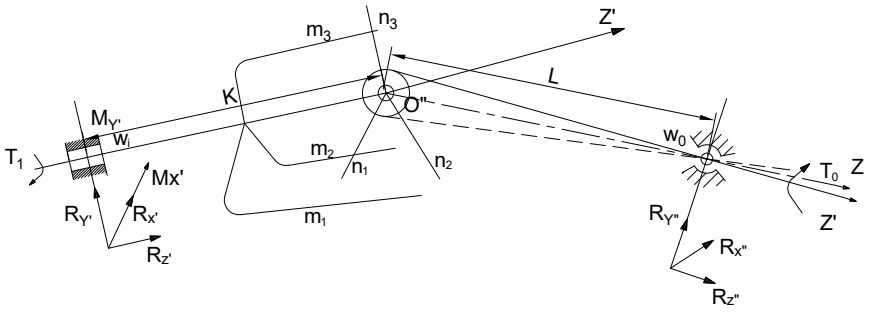

Figure 7. The kinetics abbreviated drawing of a tripod universal joint with a self-align bearing.

Preprints.org (www.preprints.org) | NOT PEER-REVIEWED | Posted: 5 March 2024 doi:10.20944/preprints202403.0252.v1

Based on the motion analysis, it is known that this type of coupling achieves quasi-constant angular velocity transmission [15]. Therefore, we can set $\omega_i \approx \omega_0 = \omega$. Additionally, considering the acceleration of the plunger sliding within the plunger groove [17], the sum of the accelerations of the three plungers is given by:

$$a_1 + a_2 + a_3 = -6\omega^2 \rho \sin\beta \cos 3\phi \tag{20}$$

$$h_i = r - \rho - 2\rho\cos 2\left(\varphi + i\frac{2\pi}{3}\right) \tag{21}$$

One end of the three-bar sliding universal joint system is mounted with a general rotary bearing, while the other end is mounted with a self-aligning bearing, belonging to a single closed spatial mechanism. The balance equations can be directly formulated. The input end is mounted with a general bearing, which can be simplified as a single pair of rotations. It lacks the constraint reaction torque along the axis of rotation and the support point is subjected to constraint reaction forces $R_{x'}, R_{y'}, R_{z'}$, and two constraint reaction torques $M_{x'}, M_{y'}$ in three directions. The ball joint connecting the input shaft and the output shaft is actually a spherical pair, transmitting forces in three directions without bearing torque. The output end is installed with a self-aligning ball bearing, which allows a spatial rotational range of $1.5° \sim 3°$. The support point does not have supporting reaction torque on the output shaft and can be simplified as a spherical pair, only bearing three support reaction forces $R_{x''}, R_{y''}, R_{z''}$ in three directions.

(1) Determining the support reaction forces for the output end with a self-aligning bearing.

The force diagram of the output shaft is as follows:

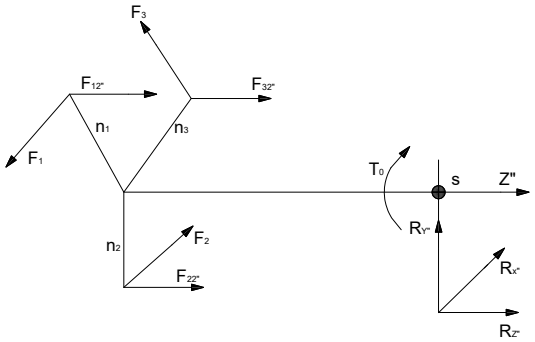

Figure 8. the kinetic abbreviated drawing of the tripod universal joint's output axle.

When neglecting friction, the force acting on the three-bar by the ball joint can be decomposed into a force F perpendicular to the three-bar in plane $X''O''Y''$ and a force $F_{Z''}$ along axis Z''. There is a resisting torque T0 acting on the output shaft, as shown in the figure above. By torque equilibrium, we can obtain:

$$F_1 \cdot h_1 + F_2 \cdot h_2 + F_3 \cdot h_3 + = T_0 \tag{22}$$

The components of force F along the X'', Y'' directions in plane $X''O''Y''$ can be determined from the diagram below:

Preprints.org (www.preprints.org) | NOT PEER-REVIEWED | Posted: 5 March 2024 doi:10.20944/preprints202403.0252.v1

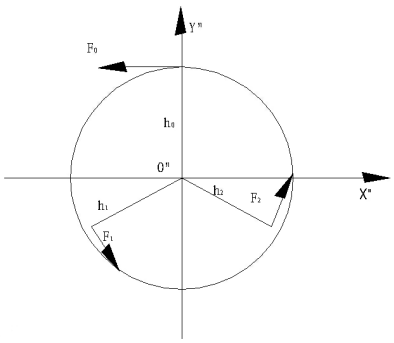

Figure 9. the pictorial drawing of the twisting forces on the tripod.

$$\begin{cases} F_{3x''} = -F_3 \sin\phi \\ F_{3y''} = F_3 \cos\phi \end{cases} \begin{cases} F_{1x''} = -F_1 \sin\left(\phi + \dfrac{2\pi}{3}\right) \\ F_{1y''} = F_1 \cos\left(\phi + \dfrac{2\pi}{3}\right) \end{cases} \begin{cases} F_{2x''} = -F_2 \sin\left(\phi + \dfrac{4\pi}{3}\right) \\ F_{2y''} = F_2 \cos\left(\phi + \dfrac{4\pi}{3}\right) \end{cases} \tag{23}$$

When considering , the moments of each component force about point S are taken. Because point S is supported by a spherical pair, there are no support reaction moments, so:

$$M_{x''} = 0 \qquad M_{y''} = 0$$

Attainable

$$F_1 = F_2 = F_3 = F = \frac{T}{h_1 + h_2 + h_3} = \frac{T_0}{3r - 3\rho} \tag{24}$$

Force equilibrium equation for the output shaft.

$$\left.\begin{aligned} R_{x''} + F_{1x''} + F_{2x''} + F_{3x''} = 0 \\ R_{y''} + F_{1y''} + F_{2y''} + F_{3y''} = 0 \\ R_{z''} + F_{1z''} + F_{2z''} + F_{3z''} = 0 \end{aligned}\right\} \tag{25}$$

The support reaction force of the output shaft bearing can be obtained from equation (23).

$$\left.\begin{aligned} R_{x''} = 0 \\ R_{y''} = 0 \\ R_{z''} = -F_{1z''} - F_{2z''} - F_{3z''} \end{aligned}\right\} \tag{26}$$

The results show that the restraining forces $R_{x''}, R_{y''}$ on axes X'' and Y'' at the output end of the spherical roller bearing are both zero, leaving only the restraining force $R_{z''}$ on axis Z'' unknown. According to the principle of action and reaction, the forces $F_{x''}, F_{y''}, F_{z''}$ acting on the triple rod are transformed into the $OX'Y'Z'$ coordinate system, and should be equal in magnitude but opposite in direction to the forces $F_{x'}$ $F_{y'}$ $F_{z'}$ acting on the ball joints connected to the piston. Consequently:

$$\begin{bmatrix} F_{x'} \\ F_{y'} \\ F_{z'} \end{bmatrix} = -[C_{o'o''}] \begin{bmatrix} F_{x''} \\ F_{y''} \\ F_{z''} \end{bmatrix} \tag{27}$$

 doi:10.20944/preprints202403.0252.v1

In the above equation, the following are known:

$$F_{z'}=ma_i, F_{x''}=-F\sin\left(\varphi+i\frac{2\pi}{3}\right), F_{y''}=F\cos\left(\varphi+i\frac{2\pi}{3}\right)(i=0,1,2) \tag{28}$$

m represents the mass of the piston rod, and a_i represents the acceleration of the piston. The unknown parameters are $F_{x'}, F_{y'}, F_{z''}$. Expanding the equation results in three equations with three unknowns, therefore, equation (27) can be solved. Among them:

$$[C_{O'O''}]=\begin{bmatrix} A_1 & A_2 & A_3 \\ B_1 & B_2 & B_3 \\ C_1 & C_2 & C_3 \end{bmatrix}$$

Among them [17]:

$$A_1=\cos\beta\cos\theta_y-\frac{\sin\beta\sin 2\theta\cos 3\varphi_0}{2\cos\theta_y} \quad A_2=-\frac{\sin\beta\sin\theta\sin 3\varphi_0}{\cos\theta_y}$$

$$A_3=-\cos\beta\sin\theta\cos 3\varphi_0-\sin\beta\cos\theta$$

$$B_1=-\frac{\sin^2\theta\sin 6\varphi_0}{2\cos\theta_y} \quad B_2=\frac{\cos\theta}{\cos\theta_y} \quad B_3=-\sin\theta\sin 3\varphi_0$$

$$C_1=\sin\beta\cos\theta_y+\frac{\cos\beta\sin 2\theta\cos 3\varphi_0}{2\cos\theta_y} \quad C_2=\frac{\cos\beta\sin\theta\sin 3\varphi_0}{\cos\theta_y}$$

$$C_3=-\sin\beta\sin\theta\cos 3\varphi_0+\cos\beta\cos\theta$$

Expanding equation (27), we get:

$$\begin{cases} F_{x'}=-A_1F_{x''}-A_2F_{y''}-A_3F_{z''} \\ F_{y''}=-B_1F_{x''}-B_2F_{y''}-B_3F_{z''} \\ F_{z'}=-C_1F_{x''}-C_2F_{y''}-C_3F_{z''} \end{cases} \tag{29}$$

Substitute equation (28) into the third equation of equation (29) to obtain.

$$F_{iz''}=-\left(\frac{ma_i}{C_3}-\frac{C_1}{C_3}F\sin\left(\varphi+i\frac{2\pi}{3}\right)+\frac{C_2}{C_3}F\cos\left(\varphi+i\frac{2\pi}{3}\right)\right) \qquad (i=0,1,2)$$

Therefore, using formula (20) and omitting term , substituting C3 simplifies to:

$$R_{Z''}=-6m\rho\omega^2 tg\beta\cos 3\varphi \tag{30}$$

Preprints.org (www.preprints.org) | NOT PEER-REVIEWED | Posted: 5 March 2024 doi:10.20944/preprints202403.0252.v1

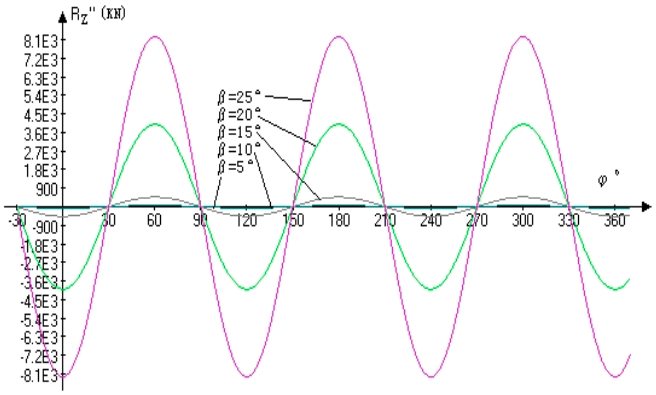

Figure 10. the relation curves of $R_{Z''}$-φ when the β angle is been different value.

When taking m=0.2Kg, $\frac{2000\pi}{60}$ in radians per second, $r = 26mm$, $l = 700mm$, $R_{Z''}$ changing with φ as shown in the figure above. As the output shaft rotates one cycle, the axial force exhibits three periods of variation with six zero-crossings. When β =0, $R_{Z''}$ =0; when $\beta = 5°, \beta = 10°$, the axial force almost coincides with the abscissa and can even be neglected; when $\beta \le 20°$, the peak value of the axial force increases slowly; when $\beta \ge 25°$, the peak value of the axial force sharply rises, reaching over 8000 kilonewtons, increasing the system's instability, which should be overcome, while the periodic axial force variation will cause the system to generate judder and longitudinal vibration.

The method to simultaneously solve for $F_{ix'}$、$F_{iy'}$ is as follows:

$$\left.\begin{aligned} F_{ix'} &= A_1 F\sin\left(\varphi + i\frac{2\pi}{3}\right) - A_2 F\cos\left(\varphi + i\frac{2\pi}{3}\right) + A_3\left[\frac{ma_i}{C_3} - \frac{C_1}{C_3}F\sin\left(\varphi + i\frac{2\pi}{3}\right)\right. \\ &\quad \left. + \frac{C_2}{C_3}F\cos\left(\varphi + i\frac{2\pi}{3}\right)\right] \\ F_{iy'} &= B_1 F\sin\left(\varphi + i\frac{2\pi}{3}\right) - B_2 F\cos\left(\varphi + i\frac{2\pi}{3}\right) + B_3\left[\frac{ma_i}{C_3} - \frac{C_1}{C_3}F\sin\left(\varphi + i\frac{2\pi}{3}\right)\right. \\ &\quad \left. + \frac{C_2}{C_3}F\cos\left(\varphi + i\frac{2\pi}{3}\right)\right] \end{aligned}\right\}(i = 0,1,2) \tag{31}$$

(2) Determining the support reaction of the input shaft bearing.

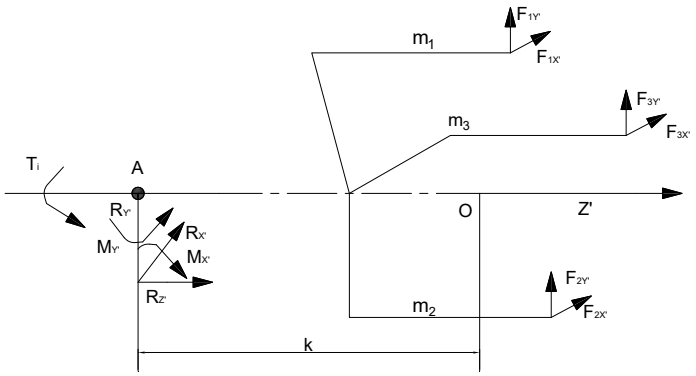

Figure 11. the kinetics abbreviated drawing of the tripod universal joint's input axle.

Preprints.org (www.preprints.org) | NOT PEER-REVIEWED | Posted: 5 March 2024 doi:10.20944/preprints202403.0252.v1

Ignoring friction, the force applied to the ball joint due to the trine is determined by the above calculation. The component along the Z' axis generates acceleration of the plunger without affecting the input shaft. Therefore, for now, the interaction between the plunger and the input shaft is not considered, and they are treated as a whole to address the force problem of the system (the force component in the Z' direction can be considered as 0). Three force equilibrium equations can be established for spatial mechanisms.

$$\begin{cases} \sum F_{x'} = R_{x'} + F_{1x'} + F_{2x'} + F_{3x'} = 0 \\ \sum F_{y'} = R_{y'} + F_{1y'} + F_{2y'} + F_{3y'} = 0 \\ \sum F_{z'} = R_{z'} + 0 = 0 \end{cases} \tag{32}$$

Substitute equation (31) into equation (32) and solve to obtain:

$$R_{x'} = tg\beta m\left(a_1 + a_2 + a_3\right) = -6m\omega^2\rho\sin\beta tg\beta\cos 3\varphi \tag{33}$$

Same:

$$R_{y'} = -\frac{1}{l}\left(3m\rho^2\omega^2 tg\beta\sin 6\varphi\right) \tag{34}$$

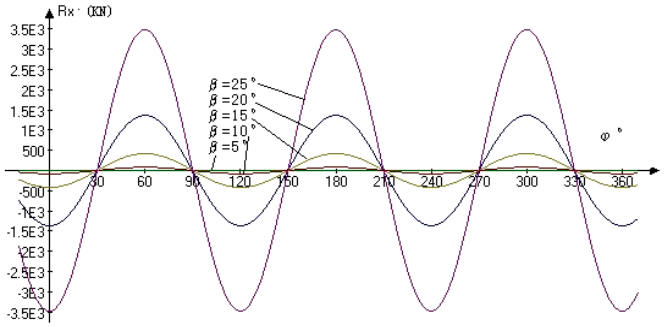

Figure 12. the relation curves of $R_{x'} - \varphi$ when the β angle is been different value.

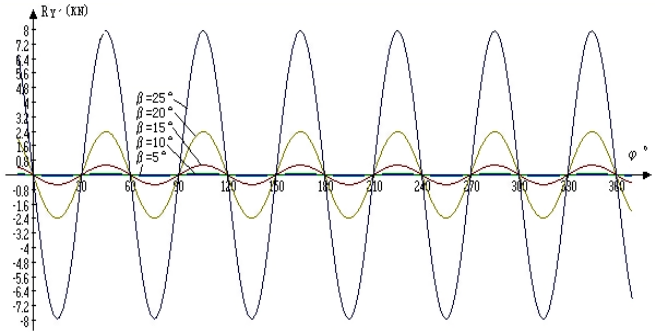

Figure 13. the relation curves of $R_{Y'} - \varphi$ when the β angle is been different value.

From the above results, it can be observed that both $R_{x'}$ and $R_{y'}$ undergo periodic changes during the motion process. The frequency of variation for $R_{x'}$ is three times the angular frequency, while for $R_{y'}$, it is six times the angular frequency. When the β angle is the same, the peak value of is much smaller than that of . Under different β values, the variation pattern of $R_{y'}$ and $R_{y'}$ is similar to $R_{Z''}$. When $\beta = 5°,\ \beta = 10°$, the support reaction force almost coincides with the abscissa. When $\beta \geq 25^0$, due to the sharp increase in the support reaction force, very strict

 doi:10.20944/preprints202403.0252.v1

requirements are imposed on the strength and stiffness of the input shaft. If $R_{x'}$ and $R_{y'}$ are too large, significant additional bending moments will be generated, leading to higher requirements for the strength and stiffness of the input shaft, while wear and vibration are inevitable, causing damage not only to the components themselves but also increasing the kinetic energy loss of the system.

5. Conclusions

(1) Through the motion analysis of the input and output shafts, it is observed that when a triple-rod universal joint coupler is installed with a self-aligning bearing on the output shaft, there is a difference in angular displacement, indicating that the transmission of the coupler does not belong to constant angular velocity transmission. However, due to the small angular displacement difference, especially when the deflection angle is very small, the angular displacement difference is extremely tiny. Therefore, the transmission of the triple-rod universal joint coupler under such conditions can be referred to as quasi-constant angular velocity transmission.

(2) Through the analysis of the forces on the output shaft, it is observed that the magnitude of the circumferential forces transmitted by the three link rods is equal. The output shaft is subjected only to axial forces, which exhibit periodic variation. The magnitude of the axial force increases with the increase of parameter β, proportional to the square of the angular velocity. When $\beta \le 25^0$ is large, the change in axial force is slow.

(3) Through the analysis of the forces on the input shaft, it is evident that the reaction force varies periodically, increasing with the value of parameter β and proportional to the square of the angular velocity. When $\beta \ge 25^0$ is large, due to the sharp increase in the reaction force, stringent requirements are placed on the strength and rigidity of the input shaft. By appropriately increasing the length of the output shaft and reducing the length of the input shaft, the magnitude of the reaction torque can be effectively reduced, thus improving the stress state of the system.

(4) The optimal range of application angle for a three-bar universal joint coupling is $\beta \le 25^0$. At this point, the system exhibits excellent transmission and mechanical performance. By reducing the angular velocity and adjusting the relevant dimensional parameters, the applicable angle range can be further expanded.

References

1. Fan, Z.M.; Meng, Z.M. Mechanical Design Fundamentals [M]. in Beijing: Machinery Industry Press, 2016.
2. Xu, Y.T.; Yao, C.Q.; Yang, Y. Analysis of Point Contact Isothermal Elastohydrodynamic Lubrication Characteristics of a New Type of Trigeminal Universal Coupling for Automobile [J]. IoP - Institute of Physics,2023, 012011.
3. Zhu, J.L. Static Analysis of Double Universal Couplings [J]. published in the Journal of Jilin University of Technology, 1995, 25(4)；pp. 72-79.
4. Pu, L.G.; Chen, G.D. Mechanical Design [M]. in Beijing. Higher Education Press, 2013.
5. Zhao, X.H. Study on Vibration Force and Vibration Torque Balance of Spatial Mechanisms [J]. Journal of Mechanical Transmission, 1994, 18(4);pp.28-31.
6. Universal Joint and Driveshaft Design Manual. Advance In Engineering Series, (7),1979.
7. Wang, W.Y. Automobile Design [M]. in Beijing: Machinery Industry Press, 2011.
8. J.M.Roethlisberger and F.C.Aldrich, The Tri-Pot Universal Joint, SAE Paper 690257, 1969；pp. 22-26.
9. Zhou, Y.; Chang, D.G.; Li, S.M. al.Grease thermal elastohydrodynamic lubrication pro-perties of tripod sliding universal couplings [J]. Industrial Lubrication and Tribology, 2018,70(1);pp.133-139.
10. Zhou, Y.; Chang, D.G.; S.M. D L S .Analysis on grease lubrication properties of the tripod sliding universal coupling in automotive transmission shaft [J].Industrial Lubrication and Tribology, 2017, 69(4);pp.598-604.
11. Pang, F.; Chang, D.G.; Zou.Y.Y. Motion Precision Analysis of Tripod Sliding Universal Coupling [J]. Mechanical, 2003, 30(1);pp.22-26.
12. Shu, F. Theoretical study and simulation of the trunnion-ball-cage universal joint drive shaft system [J]. Journal of Mechanical & Electrical Engineerin, 2015,32(11);pp.1459-1461.

 doi:10.20944/preprints202403.0252.v1

13. Wei, J.B.; Xu.Y.T. Analysis of Torsional Vibration Characteristics of Three-Yoke- Cage-Type Double Universal Joint Couplings [J]. Journal of Engineering Design, 2021,28(4);pp.458-465.
14. Miao, X.L. Analysis of the Average Transmission Efficiency of Three-Pronged Universal Couplings [J]. Mechanical Management and Development, 2023,38(10);pp.26-28.
15. Schmelz, v.Sheerr-Thoss, Aucktor. Gelenke und Gelenkwellen. Springer-Verlag, 1988.
16. Zhang, Q.X. Analysis and Synthesis of Spatial Mechanisms, Volume I by [M]. in Beijing:published by Machinery Industry Press, 1984.
17. Li, L. Analysis of Angle Difference of Tripod Universal Coupling [J]. Journal of Qingdao Institute of Chemical Technology, 2001, 22(1);pp.74-78.
18. Li L. Calculation of Motion Parameters of Moving Pairs in Tripod Universal Couplings [J]. Mechanical Engineer, 2004, (10);pp.50-52.